

Computational Simulation of Flow Over a High Lift Trapezoidal Wing

**Abhishek Khare^a, Raashid Baig^a, Rajesh Ranjan^a, Stimit Shah^a,
S. Pavithran^a, Kishor Nikam^a and Anutosh Moitra^b**

^a Computational Research Laboratories Ltd., Pune, India

^b The Boeing Company, Seattle, USA

Abstract

Reynolds Averaged Navier-Stokes (RANS) simulations and analysis of a trapezoidal three element high lift wing, using CFD++, is presented in this paper. Parametric study of grid and solver effect has been done. Requirements of the grid refinement at critical locations of the geometry are discussed. Optimized volume stretching ratio has been identified through the grid independent study. Simulations using various turbulence models available in CFD++ with various grids have been performed and results are documented. Predicted trends of lift coefficient (C_L) and its maximum value ($C_{L_{max}}$) are in close agreement with experimental data.

1. INTRODUCTION

High-lift systems are indispensable part of commercial jet transports. These systems enable the commercial airplanes to efficiently perform their low speed operations, which further affect takeoff and landing field length, approach speed etc. Therefore efficient design of high-lift system is a critical part of the design cycle of the commercial transport airplanes. Simulating high-lift flows using computational codes is indeed a challenging task because of the complexities of the geometry and flow physics involved. For example, complex physics includes attachment line transition, relaminarization, viscous wake interactions, confluent boundary layers, separation and reattachment. Trapezoidal wing is an open domain high lift problem posed by NASA Langley Research Center (LaRC) for interested researchers to validate their CFD codes against available experimental data. The experimental data for various take-off and landing configurations for a simplified high lift wing with leading and trailing edge devices is reported by NASA LaRC.

The amount of validation that has been carried out in the past for 3D high lift flows is limited. The reasons given by Bussoletti et al. [1] for it include lack of sufficient 3D experimental high-lift data. Also the simulations that have been carried out are on simple 3D geometries.

Previous high-lift CFD simulations in three dimensions include those of Mathias et al. [2] and Jones et al. [3] who studied a simple wing with half span flap. Cao et al. [4] computed flow over a simplified Boeing 747 high-lift configuration. Mavriplis [5] [6] and Nash and Rogers [7] computed flow over the same NASA Trapezoidal Wing used in the current work.

The current CFD analysis, performed under a collaborative research agreement between Computational Research Laboratories Ltd. and The Boeing Company. The full span landing configuration (configuration-1 as listed on NASA Trapezoidal Wing website-<http://db-www.larc.nasa.gov/trapwing/Archive/>) has been taken as experimental base and commercial code CFD++ used on supercomputer Eka to perform different simulations. The work presented here describes the importance of generating grid with adequate resolution to capture the complex viscous phenomena. It is found that grid refinement at some critical locations drive the prediction of C_L at higher angle of attack. Apart from the grid refinement study, various turbulence models have been used and comparative results are documented.

2. GEOMETRY AND EXPERIMENTAL SETUP

The NASA trapezoidal wing is a three elements high-lift configuration having a single slotted flap and slat. The wing is mounted on a simple body-pod. This model is developed and tested by NASA to provide an experimental database of a high-lift system to the global CFD community. The model has

been tested on two different wind tunnels, NASA Ames 12ft Pressurized Wind Tunnel (PWT) and NASA Langley 14X22ft Subsonic Wind Tunnel (SWT). Test data was generated for the Trapezoidal Wing with three basic configurations, full span flap take-off configuration, full span flap landing configuration and part span flap landing configuration. The current simulation utilized the full-span flap landing configuration. Flap brackets have not been included in the modeled geometry. Figure 1 shows the actual picture of the Trapezoidal Wing experimental setup and Figure 2 shows the CAD model used in the present simulation.



Figure 1. Trapezoidal Wing in 12ft test section, NASA Ames

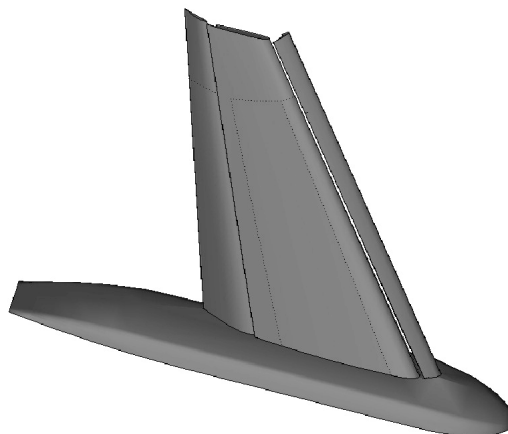


Figure 2. CAD model of the NASA Trap Wing

3. GRID GENERATION

The grid used in the present work has been generated by using Boeing's Modular Aerodynamic Design Computational Analysis Process (MADCAP) and Advancing Front Local Reconnection (AFLR3) grid generator. MADCAP is a surface grid generator which takes surfaces in various for-mats like STL, IGES etc. Geometry pre-processing and surface parameterization prior to input to MADCAP were accomplished using Boeing's System for Low-Speed Unstructured Grid Generation (SLUGG) software system. AFLR3 is a volume grid generator which takes triangulated surface grid in UGRID format and generates volume grid on that. AFLR3 generates the volume grid in two steps. In the first step it generates the viscous grid with prisms elements. Size and number of layers of prisms can be controlled by input parameters given to AFLR3. In second step of volume grid generation AFLR3 uses advancing front algorithm to fill the remaining domain with tetrahedral elements.

Surface grid at various critical regions has been refined to capture the various flow features involved. After finding out the critical regions and refining those adequately, stretching ratio (SR) has been varied to capture the wake generated from various elements and its interactions with the boundary

layers of other elements. Variable normal spacing on the surface has been used in conjunction with the thickened boundary layer. Table 1 shows the detail of the various grids used in the simulation.

Table 1. Grid details

Grid type	Surface elements	Volume elements	Stretching Ratio (SR)
A	375,680	15,860,599	1.23
B	509,089	26,612,694	1.23
C	596,872	28,143,372	1.18
D	766,841	41,730,699	1.14
E	1,036,314	69,633,564	1.10

4. SIMULATION METHODOLOGY

A compressible Reynolds Averaged Navier Stokes solver, CFD++ has been used to perform simulations. CFD++ uses cell centered, finite volume and implicit/explicit algorithms to solve the Navier Stokes equations on unstructured/structured grids. In CFD++ various topography parameter free models are used to capture turbulent flow features. The nonlinear subset of these models accounts for Reynolds stress anisotropy and streamline curvature. All turbulence models can be integrated directly to the wall or with a sophisticated wall function which accounts for compressibility as well. A rectangular domain of size 100 times the body length in all the three directions has been taken for simulations. Free stream pressure and velocity are imposed at the boundaries. Solve to wall approach has been used as the grids have been resolved to very small Y^+ (less than 1) value. Steady state simulations have been performed for all the cases. Minmod flux limiter is enabled to limit the interpolation slope in second order scheme. Convergence of the simulation depends on the turbulence model used and the angle of attack. Each simulation takes around 16 hours of wall time to complete 1000 implicit iterations on a grid size of around 28 million grid cells with 128 processors. Convergence histories of both residuals and forces were monitored.

The simulations have been performed on Eka super-computer, situated at Computational Research Laboratories, Ltd., Pune, India. Eka is a cluster of high-end compute nodes connected with high speed communications networks. With 1800 nodes, the system has a peak compute capacity of 172 teraflops and has achieved sustained compute capacity of 132.8 teraflops for the LINPACK benchmark.

5. RESULTS AND DISCUSSIONS

Simulations using various turbulence models available in CFD++ with various grids have been performed and results are discussed. Predicted trends of lift coefficient (C_L) and its maximum value (C_{Lmax}) are in close agreement with experimental data.

5.1 Turbulence Models

A baseline grid with 16 million cells has been generated on the Trapezoidal Wing with a SR of 1.23 (Grid A). Simulations for angle of attack (α) ranging from 0 to 35 degrees in steps of 5 degree have been performed. To capture C_{Lmax} , angle of attack is varied in close intervals of 1 degree between 30 to 34 degrees

The computations in the current work utilized various turbulence models (SA, KERT, SST) with the flow assumed to be fully turbulent. All baseline simulations utilized low Mach number preconditioning and were started from free-stream initial conditions. Figure 3 and 4 shows the results C_L vs. α and C_D vs. α for the baseline case. It can be seen that simulated values of C_L , C_D as well as C_{Lmax} are far below the experimental values. Results are expected to improve with better grid resolution. Viscous grid for baseline case is shown in Figure 5. Separation on the flap and near the wing body junction can be seen from the surface restricted streamlines plot shown in Figure 6.

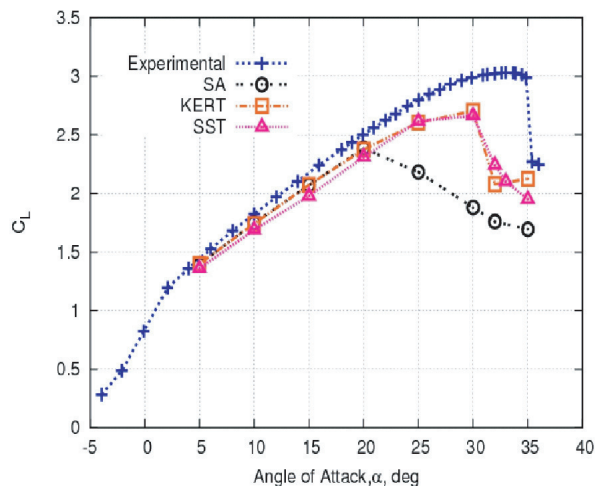


Figure 3. C_L Vs α for baseline, 16 million cells grid

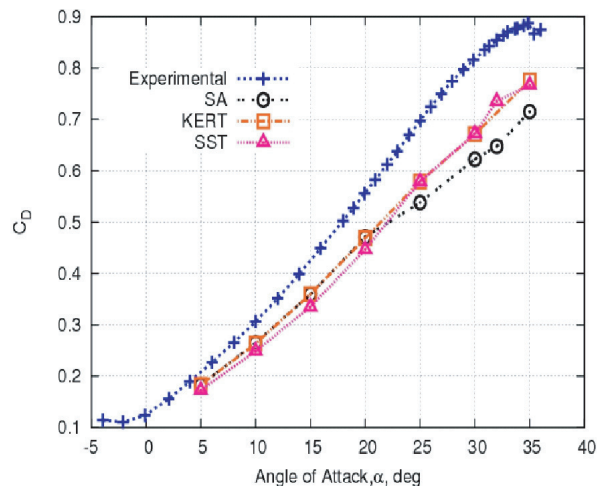


Figure 4. C_D Vs α for baseline, 16 million cells grid

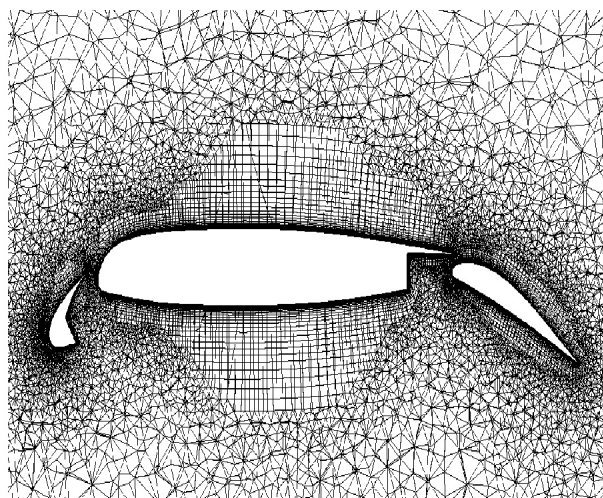


Figure 5. Grid for baseline case

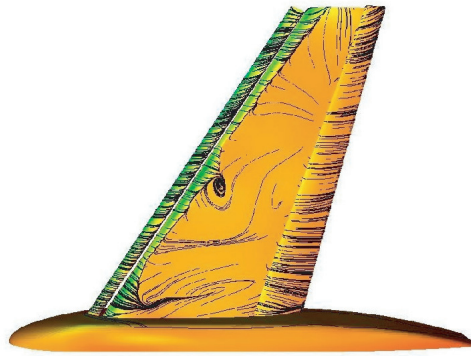


Figure 6. Surface restricted streamlines for baseline case

5.2. Effect of turbulence viscosity levels at the inlet

Specified inflow conditions for turbulence viscosity (μ_t) for the Spalart-Allmaras turbulence model have been varied and its effect on the solution is observed. Turbulent viscosity for the two cases is taken as 5 times μ and 100 times μ . No appreciable change has been observed in the results.

5.3. Surface grid density effects

For validation of any CFD simulation, study of convergence of the computed solution with increasing grid density is very important. To improve the accuracy of the computed solution, surface grid at critical locations like wing body junction, wing, flap, slat and the gaps between the elements is refined. The resulting grid B is generated with the same SR 1.23 as grid A. The consequence of refining the grid at locations mentioned above is reflected in the simulation results. This can be seen from the C_L vs. α curve in Figure 7. Surface grid refinement resulted in improvement of the linear range of the $C_L - \alpha$ curve. The effect of grid refinement on C_D is shown in Figure 8. The difference between experimental and simulation values of C_D is probably because of brackets present on the experimental geometry. Figure 9 shows the surface restricted streamlines for this case. It can be seen that flow is attached on majority of the wing as compared to baseline case. The number of cells after surface grid refinement is 26 million.

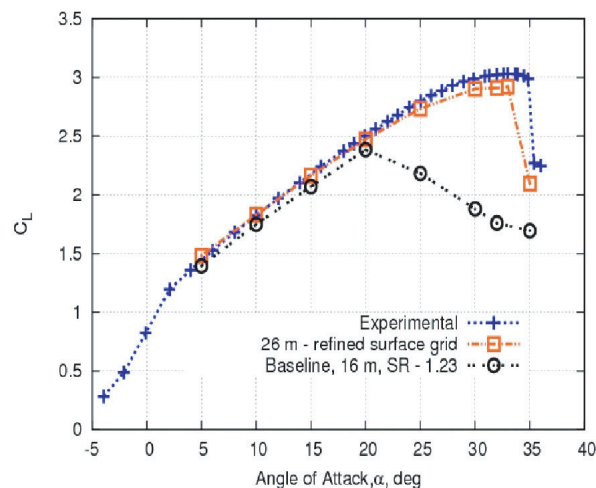


Figure 7. Comparison of C_L Vs α curves of baseline grid A with grid B

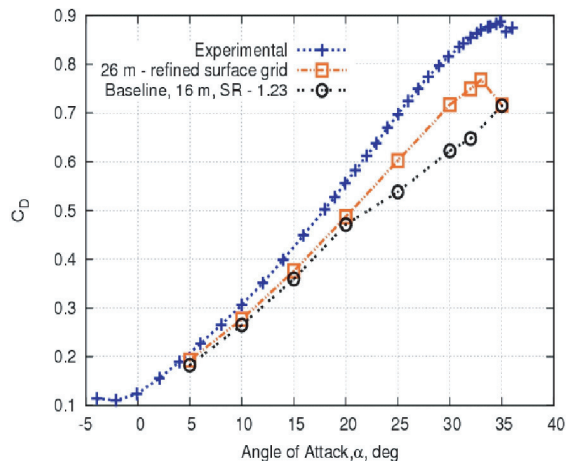


Figure 8. Comparison of C_D vs. α curves of baseline grid A with grid B

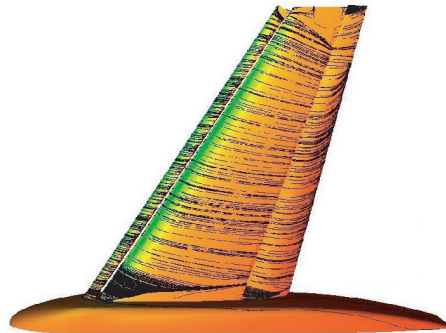


Figure 9. Surface restricted streamlines for case with grid B

5.4. Pre-conditioning Effects

For the regions where the flow-field is characterized by very low speeds, compressible flow solvers require special treatment to account for the high artificial dissipation at numerical flux. CFD++ has a general implementation of time-derivative pre-conditioning, which involves pre-multiplying the time-derivative term in the governing differential equations by a matrix which alters the rate of evolution of the physical problem. This approach arguably leads to two advantages improved convergence rates as a result of the reduced stiffness and improved accuracy as a result of the reduced dissipation. CFD++ has a provision for user to turn pre-conditioning ON or OFF, or turn it ON from a particular time step.

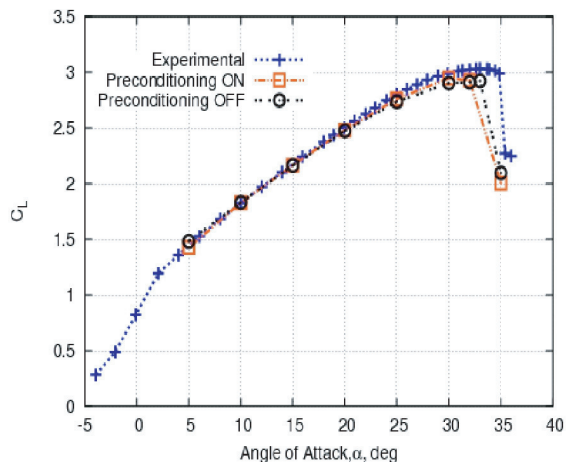


Figure 10. Pre-conditioning effects for SA model

The current case has been run with both pre-conditioning ON and OFF using SA and KERT turbulence models. As expected, no significant difference is observed between the pre-conditioned and non-pre-conditioned cases as shown in Figure 10 and 11.

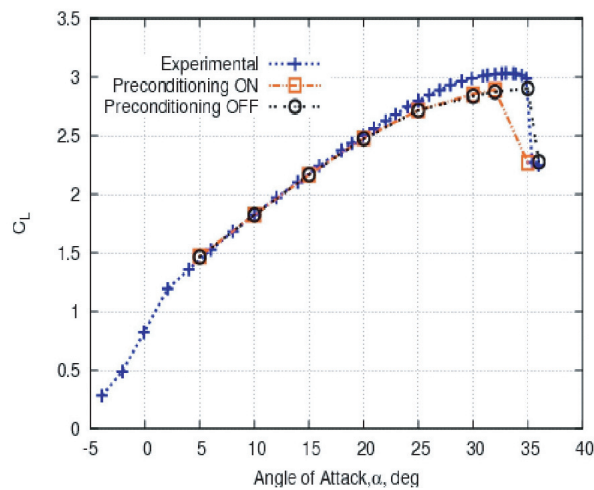


Figure 11. Pre-conditioning effects for KERT model

5.5 Effect of volume stretching ratio and variable normal spacing on surface

The interaction of the wakes and boundary layers control the physics of high lift systems. Resolution of wakes and boundary layers of varying thicknesses over geometry components of widely varying sizes is of great importance in prediction of maximum lift. The first normal distance is scaled with the location and local Reynolds number to better resolve the boundary layer. Also the boundary layer grid is thickened to capture the wake as shown in Figure 12.

Grid attributes such as normal spacing near the surface, grid density in wake regions and grid stretching ratio have large effect on the accuracy of the computed solution for complex high-lift flows. Grid stretching ratio was reduced in steps from 1.23 to 1.10 (number of cells varying from 21 million up to 70 million). These grids has been labeled as A, C, D and E as given in Table 1.

Results for C_L Vs α and C_D Vs α for the various grids have been shown in Figures 14, 15, 16 and 17. It can be seen that there is not much improvement in the results for values of SR less than 1.18 (Table 2). Results on grid C are now able to predict the linear as well as stall behavior with 2% of accuracy. In general the simulated lift curve closely resembles the experimental lift curve to engineering accuracy. Figure 13 shows surface restricted streamlines for grid C case.

It can also be observed from the results that SA turbulence model performs better compared to KERT and SST models.

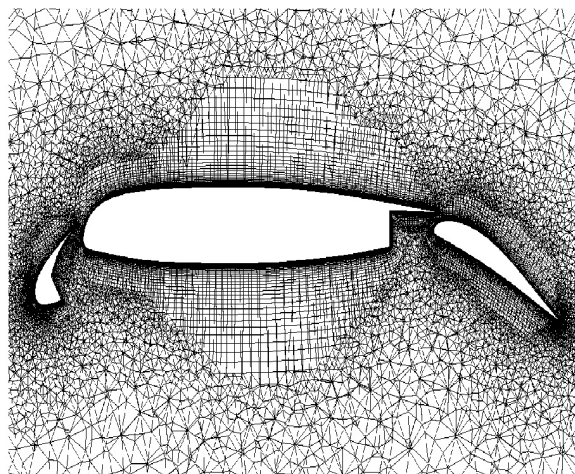


Figure 12. Grid for case with grid C

Table 2. Experimental and Simulation C_L and C_D values for SA model

Angle of Attack	10°	20°	25°	32°
Experimental C_L	1.8240	2.4997	2.7986	3.0242
Grid A (SR 1.23)	1.8069	2.4635	2.7200	2.9078
Grid C (SR 1.18)	1.8160	2.4690	2.7220	2.9380
Grid D (SR 1.14)	1.8205	2.4725	2.7272	2.9290
Grid E (SR 1.10)	1.8253	2.4779	2.7309	2.9353
Experimental C_D	0.3063	0.5557	0.6976	0.8546
Grid A (SR 1.23)	0.2719	0.4843	0.5995	0.7480
Grid C (SR 1.18)	0.2728	0.4848	0.5985	0.7529
Grid D (SR 1.14)	0.2740	0.4860	0.6001	0.7534
Grid E (SR 1.10)	0.2747	0.4867	0.5997	0.7534

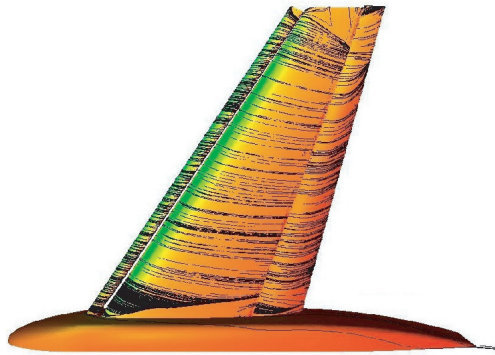
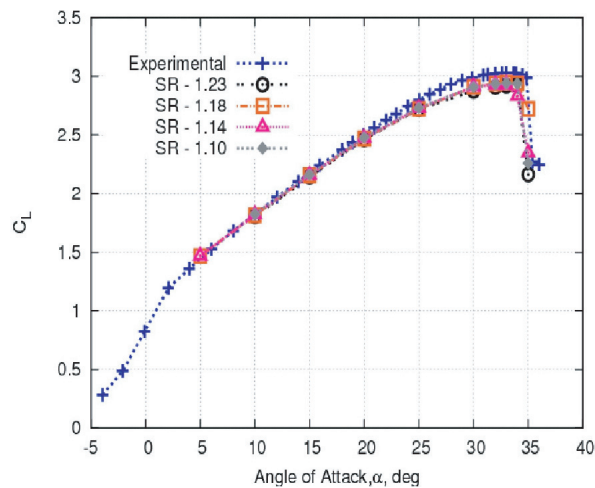


Figure 13. Surface restricted streamlines for case with grid C

Figure 14. C_L vs. α curves for different stretching ratios, SA model

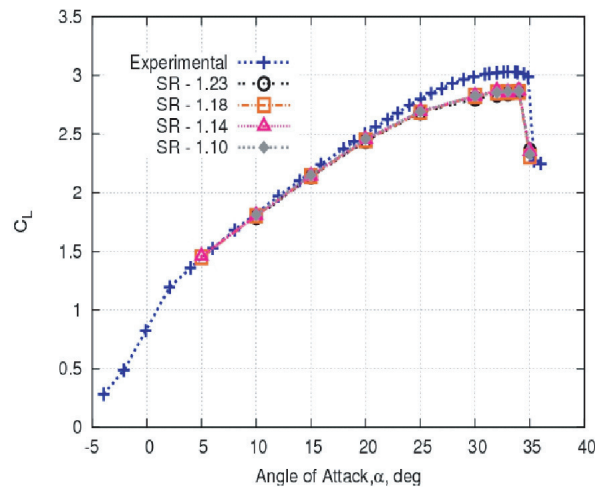


Figure 15. C_L vs. α curves for different stretching ratios, KERT model

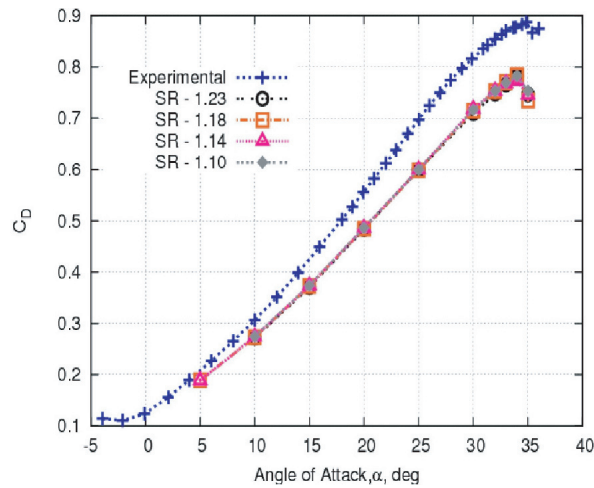


Figure 16. C_D vs. α curves for different stretching ratios, SA model

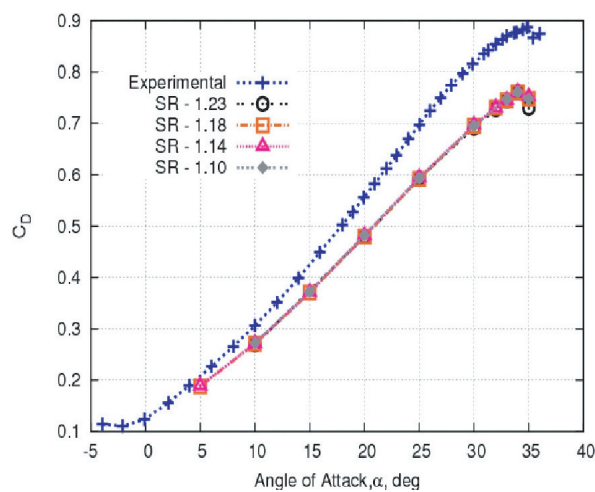


Figure 17. C_D vs. α curves for different stretching ratios, KERT model

6. SCALE-UP STUDY

Scale-up study has also been carried out for grid C (28 million cells). The efficiency of parallel implementation and speed-up have been shown in the Figures 18 and 19. The code scales up to 192 cores as can be seen. Time required for 10 implicit iterations on grid C having 28 million cells is given in Table 3.

Table 3. Time required for 10 iterations on grid C

Number of Cores	Time (in seconds)
64	533
96	364
128	299
160	281
192	274
224	279
256	363

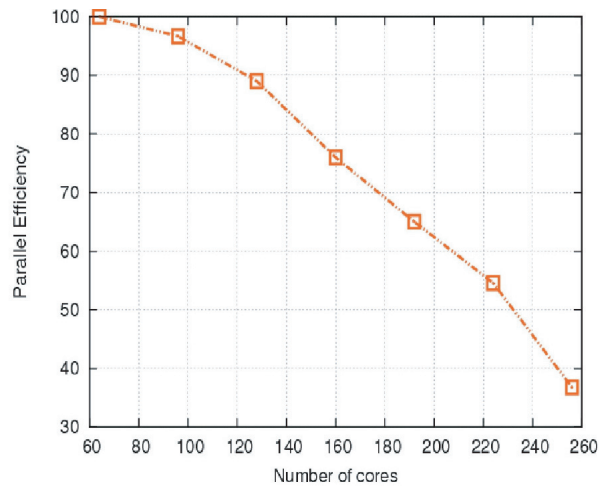


Figure 18. Efficiency of parallel implementation

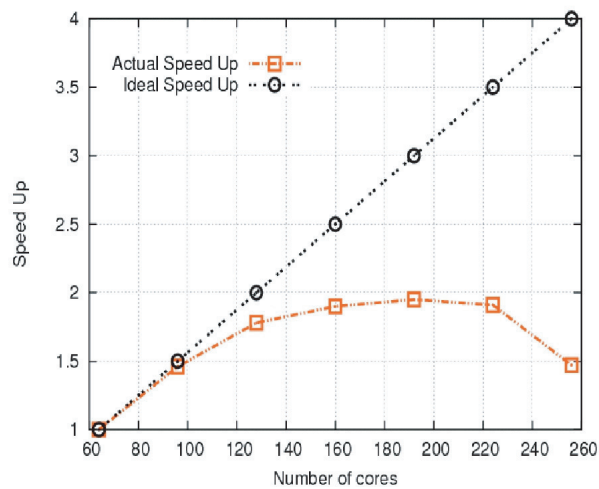


Figure 19. Scale-up study on grid C (28 million cells)

7. CONCLUSIONS

Computational simulation of high-lift NASA trap wing has been carried out using CFD++ on unstructured grids. C_{Lmax} prediction has been achieved to engineering accuracy. A systematic surface and volume grid refinement is done to capture the complex flow encountered in the high-lift system.

Various critical regions on elements have been identified for grid refinement to improve lift prediction. Grids with variable normal spacing on the surfaces have been used with different volumetric stretching ratio to capture the wakes and interactions of these wakes with the boundary layers. The simulation results of 28 million cells grid and stretching ratio 1.18 shows good match with the experimental data. Further reduction in the stretching ratio rapidly increases the number of cells without any significant improvement in the C_L vs. α curve compared with experimental values. It can be concluded that 28 million cells with SR 1.18 is sufficient if grid characteristics are right.

Although all the three turbulence models SA, KERT and SST perform well in the linear range of C_L vs. α curve, it has been observed that the SA turbulence model performs better compared to KERT and SST models in the stall range of C_L - α curve. To further improve the simulation results, unsteady simulations can be performed. Also modeling of the brackets can possibly help to improve the simulation results because of a closer match between the computational and experimental geometries.

ACKNOWLEDGEMENTS

Authors are grateful to Metacomp Technologies, Inc., USA, for their valuable support during this course of work.

REFERENCES

- [1] J. Bussioletti, P. Johnson, K. Jones, K. Roth, J. P. Slotnick, S. Ying, and S. E. Rogers, *The Role of Applied CFD within the AST/IWD Program High-Lift Subelement: Applications and Requirements*, AST/IWD Program Report, June 1996
- [2] D. L. Mathias, K. Roth, J. C. Ross, S. E. Rogers, and R. M. Cummings, *Navier-Stokes Analysis of the Flow about a Flap-Edge*, AIAA, 1995, 0185
- [3] K. M. Jones, R. T. Biedron, and M. Whitlock, *Application of Navier-Stokes Solver to the Analysis of Multielement Airfoils and Wings Using Multizonal Grid Techniques*, AIAA, 1995, 1855
- [4] H. V. Cao, S. E. Rogers, and T. Y. Su, *Navier-Stokes Analyses of a 747 High-Lift Configuration*, AIAA, 1998, 2623
- [5] D. J. Mavriplis, *Large Scale Parallel Unstructured Mesh Computations for 3D High-Lift Analysis*, AIAA, 1999, 0537
- [6] D. J. Mavriplis, *Three Dimensional Viscous Flow Analysis for High-Lift Configurations Using a Parallel Unstructured Multigrid Solver*, SAE; 1999-01-5558
- [7] S. E. Rogers, K. Roth, and S. Nash, *CFD Validation of High-Lift flows with significant wind-tunnel effects*, AIAA, 2000, 4218
- [8] A. Moitra, *Validation of an Automated CFD Tool for 2-D High-Lift Analysis*, AIAA, 2001, 2401
- [9] S. Nash, and S. E. Rogers, *Numerical Study of Trapezoidal Wing High-Lift Configurations*, SAE, 1999-01-5559
- [10] P. L. Johnson, K. M. Jones, and M. D. Madson, *Experimental Investigation of A Simplified 3D High Lift Configuration in Support of CFD Validation*, AIAA, 2000, 4217
- [11] M. S. Chaffin, and S. Pirzadeh, *Unstructured Navier-Stokes High-Lift Computations on a Trapezoidal Wing*, AIAA, 2005, 5084

